$\{Gd^{III}_7\}$ and $\{Gd^{III}_{14}\}$ Clusters Based on Rhodamine 6G Ligand with Magnetocaloric Effect

Lin Miao , Cai-Ming Liu , Hui-Zhong Kou *

Posted Date: 3 January 2024

doi: 10.20944/preprints202401.0084.v1

Keywords: lanthanide oxygen cluster; magnetocaloric effect; magnetic refrigerant materials; rhodamine ligand

Article

{Gd^{III}_7} and {Gd^{III}_{14}} Clusters Based on Rhodamine 6G Ligand with Magnetocaloric Effect

Lin Miao [1], Cai-Ming Liu [2] and Hui-Zhong Kou [1,*]

[1] Engineering Research Center of Advanced Rare Earth Materials (Ministry of Education), Department of Chemistry, Tsinghua University, Beijing 100084, P. R. China; kouhz@mail.tsinghua.edu.cn

[2] Beijing National Laboratory for Molecular Sciences, Center for Molecular Science, Institute of Chemistry, Chinese Academy of Sciences, Beijing 100190, P. R. China; cmliu@iccas.ac.cn

* Correspondence: kouhz@mail.tsinghua.edu.cn (H.-Z.K.)

Abstract: Heptanuclear {Gd^{III}_7} (complex **1**) and tetradecanuclear {Gd^{III}_{14}} (complex **2**) have been synthesized using a Rhodamine 6G ligand HL (Rhodamine 6G salicylaldehyde hydrazone) and characterized. Complex 1 has a rare disc-shaped structure, where the central Gd ion was connected to the peripheral six Gd^{III} ions via CH_3O^-/μ_3-OH^- bridges. Complex **2** has an unexpected three-layer double sandwich structure with a rare μ_6-O^{2-} ion in the center of the cluster. Magnetic studies revealed that complex **1** exhibits a magnetic entropy change of 17.4 J kg^{-1} K^{-1} at 3 K and 5 T. On the other hand, complex **2** shows a higher magnetic entropy change of 22.3 J kg^{-1} K^{-1} at 2 K and 5 T.

Keywords: lanthanide oxygen cluster; magnetocaloric effect; magnetic refrigerant materials; rhodamine ligand

1. Introduction

The exploration of new compounds in the field of coordination chemistry reveals many fascinating structures and properties. Among them, rare earth ions play an important role in the assembly of Complex polynuclear clusters [1–3]. Due to the large ion radius and the inherent ability to participate in various coordination environments, rare earth ions can promote the formation of polymetallic clusters [4–22]. Multinuclear rare earth clusters with different structural types, such as {Ln_{18}} [23], {Ln_{28}} [24], {Ln_{34}} [25], {Ln_{36}} [26], {Ln_{37}} [27], {Ln_{48}} [28], {Ln_{60}} [29], {Ln_{72}} [30], {Ln_{104}} [31], {Ln_{140}} [32], etc., were synthesized, and the largest even has {Nd_{288}} structure [33]. These polynuclear clusters usually exhibit fascinating properties, such as single-molecule magnetism [8,12,14,15,19,30], luminescence [23,24], magneto-optical properties [34] and proton conductive properties [35].

The formation of lanthanide hydroxide clusters involves the hydrolysis of lanthanide ions in the presence of ligands. The hydrolysis process leads to the formation of small lanthanide hydroxide units, which then assemble to form larger clusters. The size and structure of the clusters can be controlled by adjusting the hydrolysis conditions and the choice of ligands. The hydrolysis-induced assembly mechanism of lanthanide hydroxide clusters is still not fully understood due to the elusive coordination configurations of lanthanide ions and the limited characterization methods available. However, recent studies have made progress in determining the intermediate species and the pathways of cluster formation [22]. The formation of high-nuclearity lanthanide clusters is believed to involve the assembly of low-nuclearity subunits, which are formed through initial hydrolysis. These small units are then connected to form the final cluster structure. Understanding the formation mechanism of lanthanide hydroxide clusters is important for the development of new functional materials and applications in various fields. In addition, the interactions between rare earth centers can affect the physical properties of the clusters. The ligand framework around these ions also plays an important role in determining the geometry, stability and functionality of the obtained clusters. By adjusting the ligand design, scientists can strategically guide the self-assembly process, thus forming the required multi-core architecture.

Preprints (www.preprints.org) | NOT PEER-REVIEWED | Posted: 3 January 2024 doi:10.20944/preprints202401.0084.v1

Some Gadolinium compounds have shown excellent magnetocaloric properties [36–38], such as $Gd(HCOO)_3$ [39], $Gd(OH)_3$ [40], $Gd_2O(OH)_4(H_2O)_2$ [40], $GdPO_4$ [41], $Gd(OH)CO_3$ [42], GdF_3 [43], $Gd(OH)F_2$ [44] and $Ba_2Gd(BO_3)_2X$ (X = F, Cl) [45]. Because the magnetocaloric effect (MCE) in Gd is particularly strong, making it an ideal material for use in extremely low temperature magnetic refrigeration systems. Magnetic refrigeration is a technology that uses a magnetic field to cool objects. Magnetic refrigeration materials are playing an increasingly important role in the future of social development, particularly in the area of energy efficiency and sustainability. In addition, molecular clusters with diverse structures also exhibit enormous magnetic cooling potential and exhibit many physical properties, such as chirality, spin crossover, fluorescence, etc.

Rhodamine-derived ligands show ring-opened or ring-closed structures and can form rare earth [46–49] or transition metals [50,51] complexes. They are most mononuclear or low-nulearity complexes. We are interested in high-nuclearity clusters based on the rhodamine ligands using the hydrolysis approach. In this work, we used the rhodamine 6G ligand (Figure 1) to synthesize two different metal complexes: hexagonal heptanuclear $\{Gd^{III}_7\}$ $[Gd_7(L)_6(\mu_2\text{-}CH_3O)_4(\mu_3\text{-}CH_3O)_4(\mu_3\text{-}OH)_4(NO_3)_2]NO_3{\cdot}10CH_3CN{\cdot}10CH_3OH{\cdot}2H_2O$ (Complex **1**) and tetradecanuclear $\{Gd^{III}_{14}\}$ $Gd_{14}(H_{0.5}L)_8(\mu_6\text{-}O)(\mu_4\text{-}O)_2(\mu_3\text{-}OH)_{16}(NO_3)_{16}{\cdot}9.5CH_3CN{\cdot}2CH_3OH{\cdot}11H_2O$ (complex **2**) with unexpected three-layer double sandwich structure. These two complexes have excellent magnetic refrigeration performance, and their magnetic entropy changes are 17.4 J kg^{-1} K^{-1} at 3 K and 5 T, and 22.3 J kg^{-1} K^{-1} at 2 K and 5 T, respectively.

2. Results and Discussion

2.1. Synthesis.

Rhodamine 6G-type ligands have attracted significant attention in the realm of fluorescent sensor. Previous studies have primarily focused on the synthesis of mononuclear rare earth or transition metal complexes [46–52]. However, these ligands have yet to be fully unearthed. We speculate that the reaction between Ln^{III} and the rhodamine 6G ligands might lead to high-nuclearity lanthanide complexes under high pH value. On the basis of the hydrolysis strategy, we have successfully synthesized two new Gd^{III} clusters **1** and **2** (Figure 1). Additionally, our research has unveiled the influential factors that impact the synthesis process, including the ratio of central ions to ligands, solvent, alkaline, and reaction temperature.

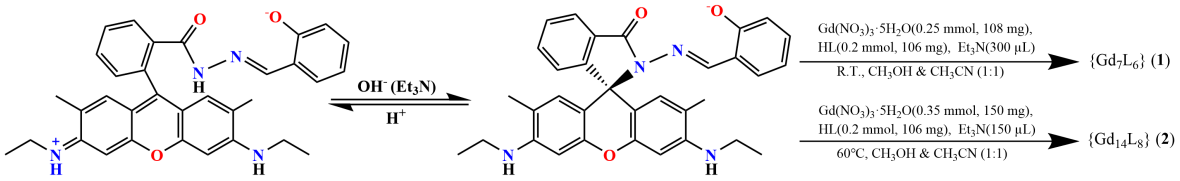

Figure 1. Transformation of ring-opened and ring-closed form of Rhodamine 6G-type ligands and its reactions.

The synthetic procedure of the two clusters is similar with the exception of the molar ratio of Gd:L, i.e. an excess amount of gadolinium nitrate was used in the synthesis of $\{Gd_{14}\}$. Both Complexes were prepared by the reaction of the ligand HL with gadolinium nitrate in a mixed solution of methanol and acetonitrile. A quantity of triethylamine was used to induce the ring close of HL and hydrolysis. The resulting mixture is left undisturbed at room temperature for one week, facilitating formation of yellow plate-like single crystals for $\{Gd_7\}$. The reactant mixture was heated at 60°C in an oven for three days, resulting in the formation of yellow, cubic-shaped samples of $\{Gd_{14}\}$. These two Complexes tend to lose solvents in the air. When the crystals are taken out of the solution, they turn from yellow to red at room temperature, and they lose the crystallinity. The powder XRD pattern of Gd_7 illustrates that the main strong peaks show disagreement with that simulated, indicating the desolvation of the crystals (Figure S1). The peaks at low 2θ angles of PXRD data for Gd_{14} are approximately consistent with that simulated.

Preprints (www.preprints.org) | NOT PEER-REVIEWED | Posted: 3 January 2024 doi:10.20944/preprints202401.0084.v1

2.2. Structure

A yellow single crystal of complex 1 was selected for single crystal X-ray diffraction at 100 K. Complex **1** crystallizes in the monoclinic system with the $P2_1/n$ space group. The volume of the unit cell is very large with a monoclinic system, and therefore the diffraction data are not so good. The command MASK was used during the structural refinement, and 452 electrons were masked per formula unit which account for the missing NO_3^- anion, 10 acetonitrile, 10 methanol and 2 H_2O molecules with the total electrons of 451. The crystallographic data and selected bond distances and angles are given in Tables S1 and S2. The asymmetric unit cell contains three crystallographically independent $\{Gd^{III}_7\}$ moieties. Because they have similar molecular structures, only one of them is described in detail as a representative. The coordination number of each Gd^{III} ion in $\{Gd_7\}$ (Figure 2) is between 7 and 9. Their coordination patterns are shown in Figures S2 and S3. Using SHAPE software for calculation, their coordination patterns were obtained as shown in Tables S3–S5. The central Gd1 ions are coordinated by eight oxygen atoms and have a square antiprism structure D_{4d}. Among the eight oxygen atoms, four are μ_3-OH^- and another four are μ_3-CH_3O^-. The remaining six Gd^{III} ions are evenly distributed around the central Gd^{III} ion, forming a saddle-shaped structure, which is relatively rare in rare earth complexes [53] (Figure S4). One ring-closed ligands L^- is coordinated to one peripheral Gd^{III} ion, and adjacent Gd^{III} ions are bridged by CH_3O^-/μ_3-OH^- and/or phenoxy oxygen atoms as shown in Figure 3.

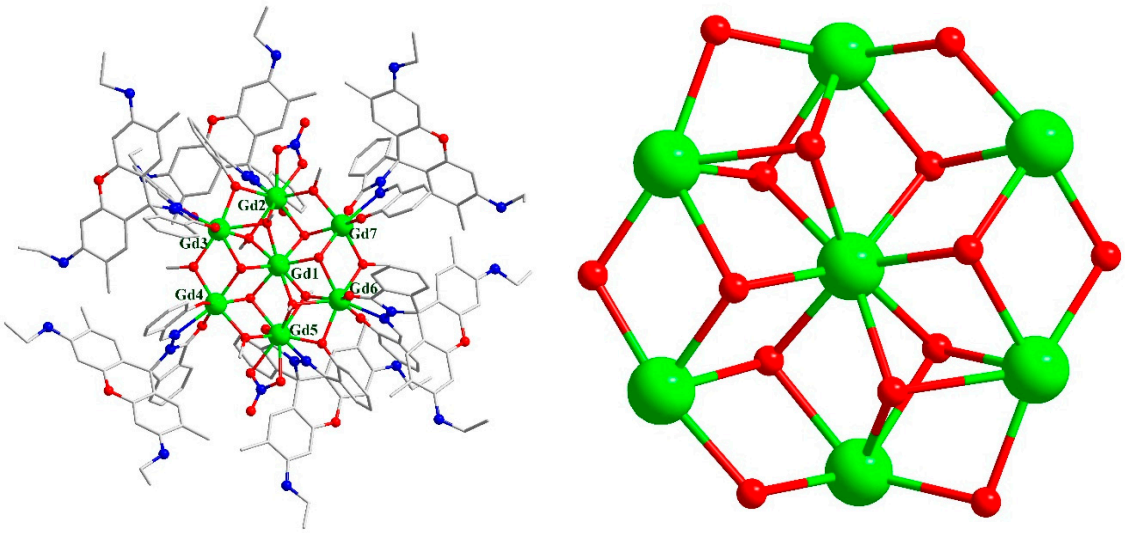

(**a**) (**b**)

Figure 2. (**a**) The structure of $\{Gd^{III}_7\}$ cation for complex **1**. Hydrogen atoms and solvents have been omitted for clarity. (**b**) The core skeleton graph of complex **1**. Color code: Gd^{III} green; O red; N blue; C grey.

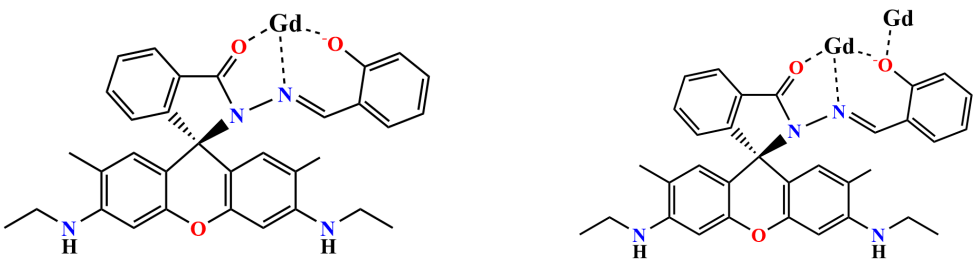

(**a**) (**b**)

Figure 3. Schematic diagram of two different coordination modes of ring-closed Rhodamine ligands L^-. (**a**) Tridentate chelating mode; (**b**) Phenolic oxygen bridging mode.

Preprints (www.preprints.org) | NOT PEER-REVIEWED | Posted: 3 January 2024 doi:10.20944/preprints202401.0084.v1

As for complex **2**, a yellow cube single crystal was selected for single crystal X-ray diffraction at 100 K. A solvent mask was used and 183.4 electrons were found in a volume of 3448.9 Å^3 in 9 voids per unit cell, which is consistent with the presence of 2 CH_3OH, 2 H_2O and 1.5 CH_3CN per formula unit with 178 electrons. The crystalographic data and selected bond distances and angles are given in Tables S1 and S6. Complex **2** crystallizes in the tetragonal system with space group of *P*4/n and has a D_{4h} symmetry. The asymmetric unit contains 1/4 of the tetradecanuclear molecule and there are five different kinds of Gd^{III} ions (Gd1-Gd5, Figure 4b). They have three different coordination modes (Table S7), and their coordination patterns are shown in the Figures S5 and S6. The tetradecanuclear cluster core is neutral, and has a highly symmetrical three-layer double sandwich structure (Figure 4b). In the structure, four nine-coordinated Gd^{III} ions form a square plane layer, and a nine-coordinated Gd^{III} ion is located between the layers. The distance between the two layers is 5.792 Å. The center of the middle layer is six-coordinated μ_6-O^{2-}, while the outer layers on both sides are μ_4-O^{2-}. The sandwiched Gd^{III} ions and the square-shaped layer are connected by μ_3-OH^- ions. The Gd ions are linked together through hydrophilic hydroxo bridges, forming a $[Gd_{14}(\mu_6\text{-O})(\mu_4\text{-O})_2(\mu_3\text{-OH})_{16}]$ core. This core contains one octahedral $[Gd_6(\mu_6\text{-O})(\mu_3\text{-OH})_8]$ unit that shares two apexes with two $[Gd_5(\mu_4\text{-O})(\mu_3\text{-OH})_4]$ square pyramid moieties. The cluster core is surrounded by eight ring-closed L^- ligands. Additionally, the Gd^{III} of middle layer are coordinated with two nitrate ions, and Gd^{III} of outer layers on both sides are coordinated with a nitrate ion and a L^- ligand. Square plane layers are bridged by phenolic oxygen on the ligand as shown in the Figure 3b.

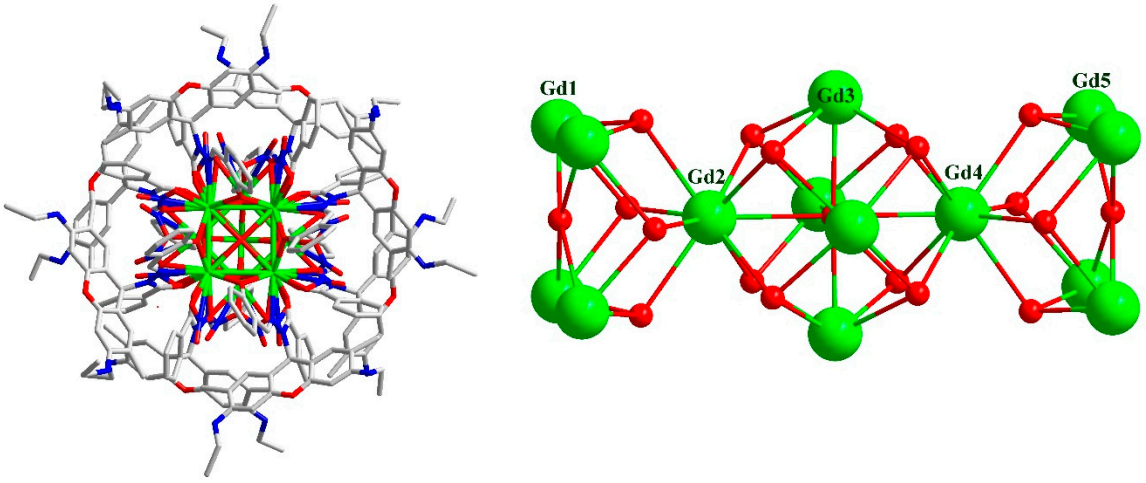

(**a**) (**b**)

Figure 4. (**a**) The structure of Complex **2**. Hydrogen atoms and solvents have been omitted for clarity.; (**b**) The core skeleton graph of Complex **2**. Color code: Gd^{III} green; O red; N blue; C grey.

Although there are many reports on tetranuclear clusters of planar quadrilateral [54,55] and nine-nuclear molecules of double-layer sandwich type [56,57], the molecular structure of rare earth in the form of a three-layer double sandwich is rare. Similar molecules have been reported before, as shown in the Figures S7–S10. The tetradecanuclear hydroxo–lanthanide acetylacetonato complexes formulated as $Ln_{14}(\mu_4\text{-OH})_2(\mu_3\text{-OH})_{16}(\mu\text{-}\eta^2\text{-acac})_8(\eta^2\text{-acac})_{16}$ (Ln = Tb and Eu, $acac^-$ = acetylacetonato) [58] and chiral tetradecanuclear hydroxo-lanthanide clusters $Ln_{14}(\mu_4\text{-OH})_2(\mu_3\text{-OH})_{16}(\mu\text{-}\eta^2\text{-acac})_8(\eta^2\text{-acac})_{16}\cdot 6H_2O$ (Ln = Dy and Tb) [59] have been reported. The ligands used in these two works are both based on acetylacetonato, but the present tetradecanuclear $\{Gd^{III}_{14}\}$ are completely different ligands, i.e. ring-closed rhodamine L^-. The use of ortho-nitrophenolate afforded the tetradecanuclear $H_{18}[Ln_{14}(\mu\text{-}\eta^2\text{-o-}O_2N\text{-}C_6H_4O)_8(\eta^2\text{-o-}O_2N\text{-}C_6H_4O)_{16}(\mu_4\text{-O})_2(\mu_3\text{-O})_{16}]$ (Ln = Dy and Tm; $o\text{-}O_2N\text{-}C_6H_4O^-$ = o-nitrophenolate) [60]. Despite the above similar Ln_{14} complexes, the μ_6-O^{2-} in **2** is unique among them.

It is worth mentioning that similar hexadecanuclear molecules $[Eu^{III}_{16}(tfac)_{20}(CH_3OH)_8(\mu_3\text{-OH})_{24}(\mu_6\text{-O})_2]$ have also been reported based on trifluoroacetylacetone ($tfac^-$) [22]. In addition to the

Preprints (www.preprints.org) | NOT PEER-REVIEWED | Posted: 3 January 2024 doi:10.20944/preprints202401.0084.v1

tetradecanuclear {Eu_{14}}, there is another two Eu ions on opposite sides. The study provides insights into the formation, evolution, and assembly of lanthanide hydroxide clusters. The formation of {Gd_7} and {Gd_{14}} in this work further verifies that the hydrolysis under high pH values is an effective way of constructing high-nuclearity Ln^{III} species.

2.3. Magnetic Measurements.

The temperature dependence of the magnetic susceptibility of Complexes **1** and **2** are measured under a 1000 Oe magnetic field in the range of 2–300 K (Figure 5). At room temperature, the $\chi_M T$ value of 54.1 cm^3 K mol^{-1} for {Gd_7} and 109.0 cm^3 K mol^{-1} for {Gd_{14}} is close to the theoretical value of 55.09 cm^3 K mol^{-1} for heptanuclear and 110.18 cm^3 K mol^{-1} for tetradecanuclear uncoupled Gd^{III} (S = 7/2, g = 2, C = 7.87 cm^3 K mol^{-1} per Gd), respectively. For **1**, upon lowering the temperature, the $\chi_M T$ value slightly decreases to 49.76 cm^3 K mol^{-1} at 20 K and then rapidly falls to 30.22 cm^3 K mol^{-1} at 2 K. 2 exhibits a similar behavior: when lowering the temperature, the $\chi_M T$ value slightly decreases to 95.4 cm^3 K mol^{-1} at 30 K and then rapidly falls to 33.0 cm^3 K mol^{-1} at 2 K. These changes indicate the presence of dominant antiferromagnetic interactions between the Gd^{III} ions in the clusters. The data can be perfectly fitted to the Curie-Weiss law, giving C = 54.44 cm^3 K mol^{-1} and θ = -1.712 K for {Gd_7} and C = 110.50 cm^3 K mol^{-1} and θ = -4.629 K for {Gd_{14}}. Larger absolute θ value in {Gd_{14}} suggests that the antiferromagnetic interaction is stronger than that for {Gd_7} (Figure S11).

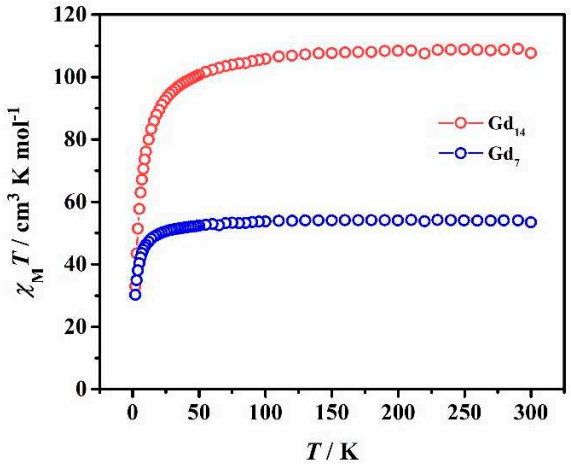

Figure 5. Temperature dependence of $\chi_M T$ for {Gd_7} and {Gd_{14}} under a 1000 Oe magnetic field in the range of 2–300 K.

The field dependence of the magnetizations (M) for Complexes **1** and **2** was measured in the temperature range of 2 - 10 K (Figure S12). It can be seen that the magnetization has not reached to saturation at 5 T and 2 K. At 2 K, the experimental maximum magnetization value of 47.03 Nβ for **1** and 89.35 Nβ for **2** is lower than the theoretical saturation value of Gd^{III} (49 Nβ for **1** and 98 Nβ for **2**, respectively), which may be owing to the antiferromagnetic coupling and higher magnetic field is needed to suppress the magnetic coupling effect. For complexes **1** and **2**, the experimental M-H curves at 2 K lie below the calculated Brillouin curve for non-interacting S_{Gd} spins (Figure S12), also suggesting the presence of intermetallic antiferromagnetic coupling. The difference between the experimental and the calculated ones for Gd_{14} is obviously larger than that for Gd_7, indicating that the former shows stronger antiferromagnetic coupling than that of the latter. The presence of μ_6-O^{2-}-bridged Gd_6O moiety may be responsible for this.

The half-filled 4f electronic configuration in a Gd^{III} ion makes it magnetically isotropic. This makes gadolinium a valuable material in various applications, especially magnetic refrigeration. Thus, the magnetocaloric effect (MCE) of Complexes **1** and **2** was studied using the Maxwell equation:

$$\Delta S_m(T)_{\Delta H} = \int [\frac{\partial M(T,H)}{\partial T}]_H \, dH$$

Preprints (www.preprints.org) | NOT PEER-REVIEWED | Posted: 3 January 2024 doi:10.20944/preprints202401.0084.v1

At 3 K and ΔH = 5 T, the value of ΔS_m is 17.44 J kg^{-1} K^{-1} for **1**(Figure 6a), which is slightly lower than the expected value of 14.56R (25.37 J kg^{-1} K^{-1}) calculated for 7 uncorrelated Gd^{III} using the equation $\Delta S_m = nR\ln(2S+1)$ ($R \approx 8.314$ J mol^{-1} K^{-1}). The value of ΔS_m for **2** is 22.30 J kg^{-1} K^{-1} at 2 K and ΔH = 5 T (Figure 6b), which is close to the expected value of 29.11R (28.72 J kg^{-1} K^{-1}) calculated for 14 uncorrelated Gd^{III}. To improve the magnetic refrigeration effect of gadolinium clusters [37], several approaches can be considered. Firstly, the experimental conditions can be optimized. For instance, the temperature and magnetic field can be carefully controlled to ensure the most efficient operation of the gadolinium clusters. The thermal conductivity of the environment and the pressure during the refrigeration cycle can also be adjusted to minimize energy loss. Secondly, the chemical composition of the clusters can be varied. Gadolinium can be alloyed with other metals to create compounds with different magnetic properties. Thirdly, the size of the clusters can be optimized. The optimal size will depend on the specific setup and application, but generally, smaller clusters have a higher surface-to-volume ratio, which leads to more efficient heat exchange and therefore a stronger refrigeration effect. However, too small clusters may also suffer from higher energy barriers between spin states, which can decrease the magnetic entropy change. Overall, a combination of these strategies can be used to improve the magnetic refrigeration effect of gadolinium clusters for various applications, such as cryogenic cooling of scientific instruments, temperature control in electronics, and energy-efficient refrigeration in households and industries.

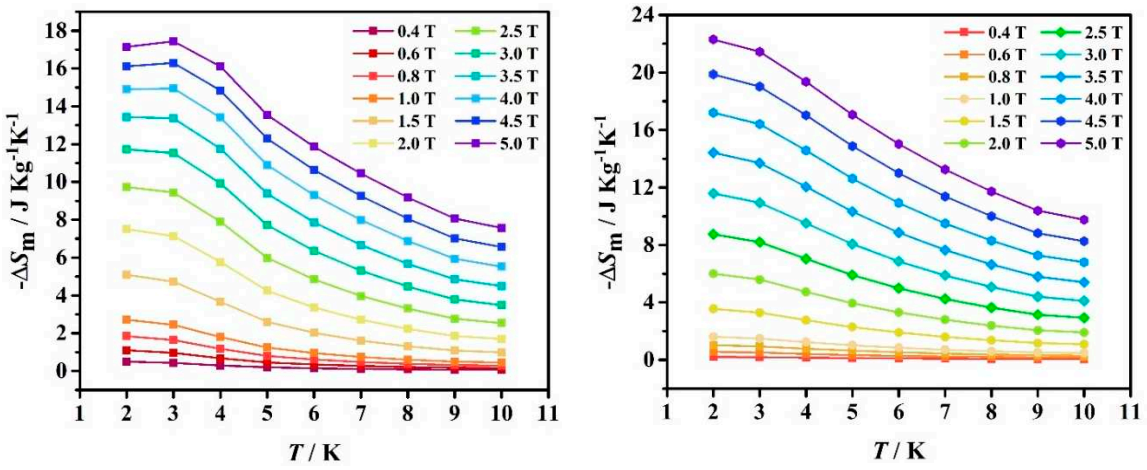

Figure 6. Experimental $-\Delta S_m$ values of **1** (a) and **2** (b) for multiple temperatures and magnetic fields calculated from magnetization data.

3. Materials and Methods

3.1. Synthesis and Preparations.

All of the reagents we used were commercially available and used without further purification. The ligand HL we used was synthesized by the literature method [46–49].

3.1.1. Synthesis of $[Gd_7(L)_6(\mu_2\text{-}CH_3O)_4(\mu_3\text{-}CH_3O)_4(\mu_3\text{-}OH)_4(NO_3)_2]NO_3\cdot 10CH_3CN\cdot 10CH_3OH\cdot 2H_2O$ (1).

The ligand HL (0.2 mmol, 106 mg) was suspended in the mixed solution of MeOH (10 mL) and MeCN (10 mL), to which $Gd(NO_3)_3\cdot 6H_2O$ (0.25 mmol, 108 mg) was added affording a red solution. The solution was heated and stirred for a few minutes, then triethylamine (300 μL) was add to give a yellow solution. The mixture was filtered, and the filtrate was placed undisturbed at room temperature. Yellow crystals suitable for X-ray diffraction analysis were collected after about 7 days. Yield: about 20%. Desolvated samples were used for elemental analysis and physical measurements. Elemental analysis calcd (%) for $C_{206}H_{214}N_{27}O_{39}Gd_7$ (4793.23): C, 51.62; H, 4.50; N, 7.89. Found: C, 51.79; H, 4.91; N, 7.92.

 doi:10.20944/preprints202401.0084.v1

3.1.2. Synthesis of $Gd_{14}(H_{0.5}L)_8(\mu_6\text{-}O)(\mu_4\text{-}O)_2(\mu_3\text{-}OH)_{16}(NO_3)_{16}\cdot 9.5CH_3CN\cdot 2CH_3OH\cdot 11H_2O$ (2).

The ligand HL (0.2 mmol, 106 mg) was suspended in the mixed solution of MeOH (10 mL) and MeCN (10 mL). $Gd(NO_3)_3\cdot 6H_2O$ (0.35 mmol, 150 mg) was added to afford a red solution. After heating and stirring for a few minutes, triethylamine (150 μL) was add, giving rise to a yellow solution. The solution was filtered and the filtrate was heated in an oven at 60ºC. Yellow crystals suitable for X-ray diffraction analysis were obtained after about 2 days and collected. Yield: about 30%. Elemental analysis calcd (%) for $C_{285}H_{330.5}N_{57.5}O_{104}Gd_{14}$ (8427.05): C, 39.62; H, 3.95; N, 9.56. Found: C, 39.27; H, 4.10; N, 9.25.

3.2. Physical measurements.

Elemental analyses (C, H, and N) were performed on an Elementar Vario Cario Erballo analyzer. Powder X-ray diffraction (PXRD) measurements were recorded on a Bruker D8 ADVANCE X-ray diffractometer using CuKα radiation (λ = 1.54184 Å) at room temperature from 5° to 50° with sweeping speed of 10°/min. Single-crystal X-ray data were collected on a Rigaku SuperNova, Dual, Cu at zero, AtlasS2. The structure was solved by program SHELXT and refined by a full matrix least-squares method based on F2 using SHELXL-2014/7 method. Hydrogen atoms were added geometrically and refined using a riding model. Temperature- and field-dependent magnetic susceptibility measurements were carried out on a Quantum Design MPMS-XL5 SQUID magnetometer.

4. Conclusions

In conclusion, novel high-nuclearity clusters have been obtained via the hydrolysis strategy: saddle-shaped {Gd_7} and three-layer double sandwich {Gd_{14}}. Both complexes exhibit good magnetocaloric properties with the magnetic entropy changes of 17.4 J kg^{-1} K^{-1} for Gd_7 at 3 K and 5 T and 22.3 J kg^{-1} K^{-1} for Gd_{14} at 2 K and 5 T, respectively. Further work on new clusters {Ln^{III}_7} and {Ln^{III}_{14}} (Ln = Dy, Tb, Eu and Ho) are in progress in our laboratory, which maybe behave as SMMs or fluorescent materials. The combination of rare earth ions and new ligands paves the way for the discovery of new polynuclear clusters with unprecedented structures and functionalities.

Supplementary Materials: The following supporting information can be downloaded at the website of this paper posted on Preprints.org Table S1. Crystal data and refinement parameters for complex **1** and **2**; Table S2. Selected bond distances (Å) and bond angles (°) for complex **1**; Table S3. The results of coordination geometric configurations evaluated by SHAPE software for seven-coordinated Gd; Table S4. The results of coordination geometric configurations evaluated by SHAPE software for eight-coordinated Gd; Table S5. The results of coordination geometric configurations evaluated by SHAPE software for nine-coordinated Gd; Table S6. Selected bond distances (Å) and bond angles (°) for complex **2**; Table S7. The results of coordination geometric configurations evaluated by SHAPE software for nine-coordinated Gd; Figure S1. Powder diffraction pattern of complexes **1**-**2**; Figure S2. Drawings of the heptanuclear surrounding polyhedral structures; Figure S3. Drawings of the coordinate lanthanide Gd^{III} surrounding polyhedral structures; Figure S4. Structure of $[Gd_7(OH)_6(thmeH_2)_5(thmeH)(tpa)_6(MeCN)_2]^{2+}$ (Gd (purple), O (yellow), N (blue), C (skeletal), H not shown); Figure S5. Drawings of the tetradecanuclear surrounding polyhedral structures; Figure S6. Drawings of the coordinate lanthanide Gd^{III} surrounding polyhedral structures; Figure S7. A diagram showing the molecular structure of $Ln_{14}(\mu_4\text{-}OH)_2(\mu_3\text{-}OH)_{16}(\mu\text{-}\eta^2\text{-}acac)_8(\eta^2\text{-}acac)_{16}$ (Ln = Tb and Eu, $acac^-$ = acetylacetonato); Figure S8. Polyhedral representation of the structure of $Ln_{14}(\mu_4\text{-}OH)_2(\mu_3\text{-}OH)_{16}(\mu\text{-}\eta^2\text{-}acac)_8(\eta^2\text{-}acac)_{16}\cdot 6H_2O$ (Ln = Dy and Tb) cluster core; Figure S9. Solid-state structure of $H_{18}[Ln_{14}(\mu\text{-}\eta^2\text{-}o\text{-}O_2N\text{-}C_6H_4\text{-}O)_8(\eta^2\text{-}o\text{-}O_2N\text{-}C_6H_4\text{-}O)16(\mu_4\text{-}O)_2(\mu_3\text{-}O)_{16}]$ (Ln = Dy, Er, Tm, Yb; o-O_2N-C_6H_4-O = o-nitrophenolate) showing the atom labeling scheme, omitting hydrogen atoms; Figure S10. Polyhedron view of the $[Eu_{16}(tfac)_{20}(CH_3OH)_8(\mu_3\text{-}OH)_{24}(\mu_6\text{-}O)_2]$ cluster where ligands have been removed for clarity; Figure S11. Temperature dependence of $\chi_M T$ for **1** (up) and **2**(down) under a 1000-Oe magnetic field in the range of 2–300 K; Figure S12. Plots of field-dependence of the magnetization for **1**(up) and **2**(down) in the range of 2–10 K at 0 - 5 T.

Author Contributions: Conceptualization and formal analysis, L.M.; writing—original draft preparation, L.M.; writing—review and editing, supervision, project administration and funding acquisition, H.Z.K. and C.M.L.. All authors have read and agreed to the published version of the manuscript.

Funding: This research was funded by the National Natural Science Foundation of China, grant number 22271171 and 21971142.

Institutional Review Board Statement: Not applicable.

Informed Consent Statement: Not applicable.

Data Availability Statement: The data supporting reported results are available from the corresponding author.

Conflicts of Interest: The authors declare no conflict of interest.

References

1. Calvez, G.; Le Natur, F.; Daiguebonne, C.; Bernot, K.; Suffren, Y.; Guillou, O. Lanthanide-based hexa-nuclear complexes and their use as molecular precursors. *Coord. Chem. Rev.* **2017**, *340*, 134-153. https://doi.org/10.1016/j.ccr.2016.12.004.
2. Yang, X. P.; Jones, R. A.; Huang, S. M. Luminescent 4f and d-4f polynuclear complexes and coordination polymers with flexible salen-type ligands. *Coord. Chem. Rev.* **2014**, *273*, 63-75. https://doi.org/10.1016/j.ccr.2013.11.012.
3. Ferrando-Soria, J.; Vallejo, J.; Castellano, M.; Martínez-Lillo, J.; Pardo, E.; Cano, J.; Castro, I.; Lloret, F.; Ruiz-García, R.; Julve, M. Molecular magnetism, *quo vadis*? A historical perspective from a coordination chemist viewpoint. *Coord. Chem. Rev.* **2017**, *339*, 17-103. https://doi.org/10.1016/j.ccr.2017.03.004.
4. Georgopoulou, A. N.; Pissas, M.; Psycharis, V.; Sanakis, Y.; Raptopoulou, C. P. Trinuclear NiII-LnIII-NiII Complexes with Schiff Base Ligands: Synthesis, Structure, and Magnetic Properties. *Molecules* **2020**, *25* (10), 2280. https://doi.org/10.3390/molecules25102280.
5. Sheikh, J. A.; Jena, H. S.; Konar, S. Co_3Gd_4 Cage as Magnetic Refrigerant and Co_3Dy_4 Cage Showing Slow Relaxation of Magnetisation. *Molecules* **2022**, *27*, 1130. https://doi.org/10.3390/molecules27031130.
6. Chen, W.-P.; Liao, P.-Q.; Yu, Y.; Zheng, Z.; Chen, X.-M.; Zheng, Y.-Z. A mixed-ligand approach for a gigantic and hollow heterometallic cage $\{Ni_{64}RE_{96}\}$ for gas separation and magnetic cooling applications. *Angew. Chem. Int. Ed.* **2016**, *55*, 9375–9379. https://doi.org/10.1002/anie.201603907
7. Li, N. F.; Luo, X. M.; Wang, J.; Wang, J. L.; Mei, H.; Song, Y.; Xu, Y. Largest 3d-4f 196-nuclear $Gd_{158}Co_{38}$ clusters with excellent magnetic cooling. *Sci. China Chem.* **2022**, *65*, 1577-1583. https://doi.org/10.1007/s11426-022-1259-9
8. Miao, L.; Liu, M. J.; Zeng, M.; Kou, H. Z. Chiral Zn_3Ln_3 Hexanuclear Clusters of an Achiral Flexible Ligand. *Inorg. Chem.* **2023**, *62*, 12814-12821. https://doi.org/10.1021/acs.inorgchem.3c01449.
9. Zeng, M.; Hu, K. Q.; Liu, C. M.; Kou, H. Z. Heterotrimetallic $Ni_2Ln_2Fe_3$ chain complexes based on $[Fe(1\text{-}CH_3im)(CN)_5]^{2-}$. *Dalton Trans.* ***2021***, *50*, 6427-6431. https://doi.org/10.1039/d1dt00693b.
10. Jin, Y. S.; Wang, X.; Zhang, N.; Liu, C. M.; Kou, H. Z. Assembly of Hydrazine-Bridged Cyclic $Fe^{III}_4Ln^{III}_4$ Octanuclear Complexes. *Cryst. Growth Des.* **2022**, *22*, 1263–1269. https://doi.org/10.1021/acs.cgd.1c01222.
11. Tian, H. Q.; Bao, S. S.; Zheng, L. M. Cyclic Single-Molecule Magnets: From Even-Numbered Hexanuclear to Odd-Numbered Heptanuclear Dysprosium Clusters. *Eur. J. Inorg. Chem.* **2016**, *19*, 3184-3190. https://doi.org/10.1002/ejic.201600392.
12. Tian, H. Q.; Bao, S. S.; Zheng, L. M. Cyclic single-molecule magnets: from the odd-numbered heptanuclear to a dimer of heptanuclear dysprosium clusters. *Chem. Commun.* **2016**, *52*, 2314-2317. https://doi.org/10.1039/c5cc08740f.
13. Goura, J.; Walsh, J. P. S.; Tuna, F.; Chandrasekhar, V. Synthesis, structure, and magnetism of non-planar heptanuclear lanthanide(III) complexes. *Dalton Trans.* **2015**, *44*, 1142-1149. https://doi.org/10.1039/c4dt01603c.
14. Mazarakioti, E. C.; Cunha-Silva, L.; Bekiari, V.; Escuer, A.; Stamatatos, T. C. New structural topologies in 4f-metal cluster chemistry from vertex-sharing butterfly units: $\{Ln^{III}_7\}$ complexes exhibiting slow magnetization relaxation and ligand-centred emissions. *Rsc Adv.* **2015**, *5*, 92526-92530. https://doi.org/10.1039/c5ra20454b.
15. Pantelis, K. N.; Perlepe, P. S.; Grammatikopoulos, S.; Lampropoulos, C.; Tang, J. K.; Stamatatos, T. C. 4f-Metal Clusters Exhibiting Slow Relaxation of Magnetization: A $\{Dy_7\}$ Complex with An Hourglass-like Metal Topology. *Molecules* **2020**, *25*, https://doi.org/10.3390/molecules25092191.
16. Peng, J. M.; Wang, H. L.; Zhu, Z. H.; Bai, J.; Liang, F. P.; Zou, H. H. Series of the Largest Dish-Shaped Dysprosium Nanoclusters Formed by *in situ* Reactions. *Inorg. Chem.* **2022**, *61*, 6094-6100. https://doi.org/10.1021/acs.inorgchem.2c00221.
17. Lu, T. Q.; Yin, J. J.; Chen, C.; Shi, H. Y.; Zheng, J.; Liu, Z. J.; Fang, X. L.; Zheng, X. Y. Two pairs of chiral lanthanide-oxo clusters Ln_{14} induced by amino acid derivatives. *CrystEngComm* **2021**, *23*, 6923-6929. https://doi.org/10.1039/d1ce00948f .

18. Zhu, Z. H.; Peng, J. M.; Wang, H. L.; Zou, H. H.; Liang, F. P. Assembly Mechanism and Heavy Metal Ion Sensing of Cage-Shaped Lanthanide Nanoclusters. *Cell Rep. Phys. Sci.* **2020**, *1*, 100165. https://doi.org/10.1016/j.xcrp.2020.100165.
19. Tian, H. Q.; Bao, S. S.; Zheng, L. M. Cyclic single-molecule magnets: from the odd-numbered heptanuclear to a dimer of heptanuclear dysprosium clusters. *Chem. Commun.* ***2016***, *52*, 2314-2317. https://doi.org/10.1039/c5cc08740f.
20. Chesman, A. S. R.; Turner, D. R.; Moubaraki, B.; Murray, K. S.; Deacon, G. B.; Batten, S. R. Tetradecanuclear polycarbonatolanthanoid clusters: Diverse coordination modes of carbonate providing access to novel core geometries. *Dalton Trans.* **2012**, *41*, 10903-10909. https://doi.org/10.1039/c2dt31101a.
21. Sun, P.-F.; Zhang, X.-N.; Fan, C.-H.; Chen, W.-P.; Zheng, Y.-Z. Tricine-supported polyoxo(alkoxo)lanthanide cluster {Ln_{15}} (Ln = Eu, Gd, Tb) with magnetic refrigerant and fluorescent properties. *Polyoxometalates* **2023**, *2*, 9140026. https://doi.org/10.26599/POM.2023.9140026.
22. Du, M. H.; Chen, L. Q.; Jiang, L. P.; Liu, W. D.; Long, L. S.; Zheng, L. S.; Kong, X. J. Counterintuitive Lanthanide Hydrolysis-Induced Assembly Mechanism. *J. Am. Chem. Soc.* **2022**, *144*, 5653-5660. https://doi.org/10.1021/jacs.2c01502.
23. Wang, Q.; Yu, Y. T.; Wang, J. L.; Li, J. N.; Li, N. F.; Fan, X. R.; Xu, Y. Two Windmill-Shaped Ln_{18} Nanoclusters Exhibiting High Magnetocaloric Effect and Luminescence. *Inorg. Chem.* **2023**, *62*, 3162-3169. https://doi.org/10.1021/acs.inorgchem.2c04065 .
24. Wang, Q.; Lu, S. H.; Xu, L. X.; Wang, J. L.; Yu, Y. T.; Bai, X.; Mei, H.; Xu, Y. $C_2O_4^{2-}$-templated cage-shaped Ln_{28}(Ln = Gd, Eu) nanoclusters with magnetocaloric effect and luminescence. *Inorg. Chem. Front.* **2023**, *10*, 4109-4116. https://doi.org/10.1039/d3qi00743j .
25. Li, Y. L.; Wang, H. L.; Zhu, Z. H.; Liang, F. P.; Zou, H. H. Giant Crown-Shaped Dy_{34} Nanocluster with High Acid–Base Stability Assembled by an out-to-in Growth Mechanism. *Inorg. Chem.* **2022**, *61*, 10101-10107. https://doi.org/10.1021/acs.inorgchem.2c01175.
26. Wu, M.; Jiang, F.; Kong, X.; Yuan, D.; Long, L.; Al-Thabaiti, S. A.; Hong, M. Two polymeric 36-metal pure lanthanide nanosize clusters. *Chem. Sci.* **2013**, *4*, 3104–3108, https://doi.org/10.1039/c3sc50887k.
27. Zhou, Y.; Zheng, X. Y.; Cai, J.; Hong, Z. F.; Yan, Z. H.; Kong, X. J.; Ren, Y. P.; Long, L. S.; Zheng, L. S. Three Giant Lanthanide Clusters Ln_{37} (Ln = Gd, Tb, and Eu) Featuring A Double-Cage Structure. *Inorg. Chem.* **2017**, *56*, 2037–2041. https://doi.org/10.1021/acs.inorgchem.6b02714.
28. Guo, F. S.; Chen, Y. C.; Mao, L. L.; Lin, W. Q.; Leng, J. D.; Tarasenko, R.; Orendac, M.; Prokleska, J.; Sechovsky, V.; Tong, M. L. Anion-Templated Assembly and Magnetocaloric Properties of a Nanoscale {Gd_{38}} Cage versus a {Gd_{48}} Barrel. *Chem. - Eur. J.* **2013**, *19*, 14876–14885. https://doi.org/10.1002/chem.201302093.
29. Luo, X. M.; Hu, Z. B.; Lin, Q. F.; Cheng, W.; Cao, J. P.; Cui, C. H.; Mei, H.; Song, Y.; Xu, Y. Exploring the Performance Improvement of Magnetocaloric Effect Based Gd-Exclusive Cluster Gd_{60}. *J. Am. Chem. Soc.* **2018**, *140*, 11219–11222. https://doi.org/10.1021/jacs.8b07841.
30. Qin, L.; Yu, Y.-Z.; Liao, P.-Q.; Xue, W.; Zheng, Z.; Chen, X.-M.; Zheng, Y.-Z. A "Molecular Water Pipe": A Giant Tubular Cluster {Dy_{72}} Exhibits Fast Proton Transport and Slow Magnetic Relaxation. *Adv. Mater.* **2016**, *28*, 10772–10779. https://doi.org/10.1002/adma.201603381.
31. Peng, J. B.; Kong, X. J.; Zhang, Q. C.; Orendac, M.; Prokleska, J.; Ren, Y. P.; Long, L. S.; Zheng, Z.; Zheng, L. S. Beauty, symmetry, and magnetocaloric effect-four-shell keplerates with 104 lanthanide atoms. *J. Am. Chem. Soc.* **2014**, *136*, 17938–17941. https://doi.org/10.1021/ja5107749.
32. Zheng, X.-Y.; Jiang, Y.-H.; Zhuang, G.-L.; Liu, D.-P.; Liao, H.-G.; Kong, X.-J.; Long, L.-S.; Zheng, L.-S. A gigantic molecular wheel of {Gd_{140}}: a new member of the molecular wheel family. *J. Am. Chem. Soc.* **2017**, *139*, 18178–18181. https://doi.org/10.1021/jacs.7b11112.
33. Wu, Y.-L.; Li, X.-X.; Qi, Y.-J.; Yu, H.; Jin, L.; Zheng, S.-T. {$Nb_{288}O_{768}(OH)_{48}(CO_3)_{12}$}: A macromolecular polyoxometalate with close to 300 niobium atoms. *Angew. Chem., Int. Ed.* **2018**, *57*, 8572–8576. https://doi.org/10.1002/anie.201804088.
34. Liu, C.-M.; Sun R.; Hao, X.; Wang B.-W. Two Pairs of Homochiral Parallelogram-like Dy_4 Cluster Complexes with Strong Magneto-Optical Properties. *Inorg. Chem.* **2023**, *62*, 20184–20193. https://doi.org/10.1021/acs.inorgchem.3c03118.
35. Hao, J.; Geng, L.; Zheng, J. Y.; Wei, J. H.; Zhang, L. L.; Feng, R.; Zhao, J. X.; Li, Q. W.; Pang, J. D.; Bu, X. H. Ligand Induced Double-Chair Conformation Ln_{12} Nanoclusters Showing Multifunctional Magnetic and Proton Conductive Properties. *Inorg. Chem.* **2022**, *61*, 3690-3696. https://doi.org/10.1021/acs.inorgchem.1c03866
36. Gschneidner, K. A.; Pecharsky, V. K. Thirty years of near room temperature magnetic cooling: Where we are today and future prospects. *Int. J. Refrig.* **2008**, *31*, 945-961. https://doi.org/10.1016/j.ijrefrig.2008.01.004.

37. Evangelisti, M.; Brechin, E. K. Recipes for enhanced molecular cooling. *Dalton Trans.* **2010**, *39*, 4672-4676. https://doi.org/10.1039/b926030g.
38. Koskelo, E. C.; Liu, C.; Mukherjee, P.; Kelly, N. D.; Dutton, S. E. Free-Spin Dominated Magnetocaloric Effect in Dense Gd_{3+} Double Perovskites. *Chem. Mater.* **2022**, *34*, 3440-3450. https://doi.org/10.1021/acs.chemmater.2c00261.
39. Lorusso, G.; Sharples, J. W.; Palacios, E.; Roubeau, O.; Brechin, E. K.; Sessoli, R.; Rossin, A.; Tuna, F.; McInnes, E. J. L.; Collison, D.; Evangelisti, M. A Dense Metal-Organic Framework for Enhanced Magnetic Refrigeration. *Adv. Mater.* **2013**, *25*, 4653–4656. https://doi.org/10.1002/adma.201301997.
40. Yang, Y.; Zhang, Q.-C.; Pan, Y.-Y.; Long, L.-S.; Zheng, L.-S. Magnetocaloric effect and thermal conductivity of $Gd(OH)_3$ and $Gd_2O(OH)_4(H_2O)_2$. *Chem. Commun.* **2015**, *51*, 7317–7320. https://doi.org/10.1039/c5cc01254f.
41. Palacios, E.; Rodríguez-Velamazán, J. A.; Evangelisti, M.; McIntyre, G. J.; Lorusso, G.; Visser, D.; de Jongh, L. J.; Boatner, L. A. Magnetic structure and magnetocalorics of $GdPO_4$. *Phys. Rev. B: Condens. Matter Mater. Phys.* **2014**, *90*, 214423. https://doi.org/10.1103/physrevb.90.214423.
42. Chen, Y.-C.; Qin, L.; Meng, Z.-S.; Yang, D.-F.; Wu, C.; Fu, Z.; Zheng, Y.-Z.; Liu, J.-L.; Tarasenko, R.; Orendáč, M.; Prokleška, J.; Sechovský, V.; Tong, M.-L. Study of a magnetic-cooling material $Gd(OH)CO_3$. *J. Mater. Chem. A* **2014**, *2*, 9851– 9858. https://doi.org/10.1039/c4ta01646g.
43. Chen, Y.-C.; Prokleška, J.; Xu, W.-J.; Liu, J.-L.; Liu, J.; Zhang, W.-X.; Jia, J.-H.; Sechovský, V.; Tong, M.-L. A brilliant cryogenic magnetic coolant: magnetic and magnetocaloric study of ferromagnetically coupled GdF_3. *J. Mater. Chem. C* **2015**, *3*, 12206–12211. https://doi.org/10.1039/c5tc02352a.
44. Xu, Q. F.; Liu, B. L.; Ye, M. Y.; Zhuang, G. L.; Long, L. S.; Zheng, L. S. $Gd(OH)F_2$: A Promising Cryogenic Magnetic Refrigerant. *J. Am. Chem. Soc.* **2022**. *144*, 13787–13793. https://doi.org/10.1021/jacs.2c04840.
45. Chen, Y. W.; Gong, P. F.; Guo, R. X.; Fan, F. D.; Shen, J.; Zhang, G. C.; Tu, H. Improvement on Magnetocaloric Effect through Structural Evolution in Gadolinium Borate Halides $Ba_2Gd(BO_3)_2X$ (X = F, Cl). *Inorg. Chem.* **2023**, *62*, 15584-15592. https://doi.org/10.1021/acs.inorgchem.3c02139.
46. Liu, M.-J.; Yuan, J.; Tao, J.; Zhang, Y.-Q.; Liu, C.-M.; Kou, H.-Z., Rhodamine Salicylaldehyde Hydrazone Dy(III) Complexes: Fluorescence and Magnetism. *Inorg. Chem.* **2018,** *57*, 4061-4069.
47. Liu, M.-J.; Wu, S.-Q.; Li, J.-X.; Zhang, Y.-Q.; Sato, O.; Kou, H.-Z., Structural Modulation of Fluorescent Rhodamine-Based Dysprosium(III) Single-Molecule Magnets. *Inorg. Chem.* **2020,** *59*, 2308-2315.
48. Liu, M.-J.; Fu, Z.-Y.; Sun, R.; Yuan, J.; Liu, C.-M.; Zou, B.; Wang, B.-W.; Kou, H.-Z., Mechanochromic and Single-Molecule Magnetic Properties of a Rhodamine 6G Dy(III) Complex. *ACS Appl. Electron. Mater.* **2021,** *3*, 1368-1374.
49. Miao, L.; Liu, M. J.; Ding, M. M.; Zhang, Y. Q.; Kou, H. Z. A Dy(III) Fluorescent Single-Molecule Magnet Based on a Rhodamine 6G Ligand. *Inorganics* **2021**, *9*, 51. https://doi.org/10.3390/inorganics9070051.
50. Yuan, J.; Wu, S. Q.; Liu, M. J.; Sato, O.; Kou, H. Z. Rhodamine 6G-Labeled Pyridyl Aroylhydrazone Fe(II) Complex Exhibiting Synergetic Spin Crossover and Fluorescence. *J. Am. Chem. Soc.* **2018**, *140*, 9426-9433. https://doi.org/10.1021/jacs.8b00103.
51. Yuan, J.; Liu, M.-J.; Wu, S.-Q.; Zhu, X.; Zhang, N.; Sato, O.; Kou, H.-Z., Substituent effects on the fluorescent spin-crossover Fe(ii) complexes of rhodamine 6G hydrazones. *Inorg. Chem. Front.* **2019,** *6*, 1170-1176.
52. Li, Y.; Huang, W.; Yong, J.; Huang, S. D.; Li, Y. J.; Liu, Y.; Wu, D. Y. Aggregation-induced ratiometric emission and mechanochromic luminescence in a pyrene-benzohydrazonate conjugate. *New J. Chem.* **2018**, *42*, 12644-12648. https://doi.org/10.1039/c8nj01379a.
53. Sharples, J. W.; Zheng, Y. Z.; Tuna, F.; McInnes, E. J. L.; Collison, D. Lanthanide discs chill well and relax slowly. *Chem. Commun.* **2011**, *47*, 7650-7652. https://doi.org/10.1039/c1cc12252e.
54. Xu, C. Y.; Wu, Z. L.; Fan, C. J.; Yan, L. L.; Wang, W. M.; Ji, B. M. Synthesis of two lanthanide clusters Ln^{III}_4 (Gd_4 and Dy_4) with [2 x 2] square grid shape: Magnetocaloric effect and slow magnetic relaxation behaviors. *J. Rare. Earth.* **2021**, *39*, 1082-1088. https://doi.org/10.1016/j.jre.2020.08.015.
55. Wang, W. M.; Li, X. Z.; Zhang, L.; Chen, J. L.; Wang, J. H.; Wu, Z. L.; Cui, J. Z. A series of [2 x 2] square grid Ln^{III}_4 clusters: a large magnetocaloric effect and single-molecule-magnet behavior. *New. J. Chem.* **2019**, *43*, 7419-7426. https://doi.org/10.1039/c8nj04454f.
56. Baril-Robert, F.; Petit, S.; Pilet, G.; Chastanet, G.; Reber, C.; Luneau, D. Site-Selective Lanthanide Doping in a Nonanuclear Yttrium(III) Cluster Revealed by Crystal Structures and Luminescence Spectra. *Inorg. Chem.* **2010**, *49*, 10970-10976. https://doi.org/10.1021/ic1011082.
57. Petit, S.; Baril-Robert, F.; Pilet, G.; Reber, C.; Luneau, D. Luminescence spectroscopy of europium(III) and terbium(III) penta-, octa- and nonanuclear clusters with β-diketonate ligands. *Dalton Trans.* ***2009***, 6809-6815. https://doi.org/10.1039/b822883c.
58. Wang, R.; Song, D.; Wang, S. Toward constructing nanoscale hydroxo–lanthanide clusters: syntheses and characterizations of novel tetradecanuclear hydroxo–lanthanide clusters. *Chem. Commun.* **2002**, 368-369. https://doi.org/10.1039/b105969f.

59. Li, X.-L.; He, L.-F.; Feng, X.-L.; Song, Y.; Hu, M.; Han, L.-F.; Zheng, X.-J.; Zhang, Z.-H.; Fang, S.-M. Two chiral tetradecanuclear hydroxo-lanthanide clusters with luminescent and magnetic properties. *CrystEngComm* **2011**, *13*, 3643-3645. https://doi.org/10.1039/c0ce00826e.
60. Bürgstein, M. R.; Gamer, M. T.; Roesky, P. W. Nitrophenolate as a building block for lanthanide chains, layers, and clusters. *J. Am. Chem. Soc.* **2004**, *126*, 5213-5218. https://doi.org/10.1021/ja0396044.